THE JOURNAL OF PHYSICAL CHEMISTRY B

ARTICLE

pubs.acs.org/JPCB

Morphology Evolution and Structural Transformation of Solution-Processed Methanofullerene Thin Film under Thermal Annealing

Lidong Zheng, Jiangang Liu, Yan Ding, and Yanchun Han*

State Key Laboratory of Polymer Physics and Chemistry, Changchun Institute of Applied Chemistry, Chinese Academy of Sciences, and Graduate University of the Chinese Academy of Sciences, 5625 Renmin Street, Changchun 130022, People's Republic of China

ABSTRACT: The film morphology and nanostructure of the soluble fullerene, [6,6]-phenyl-C_{61} butyric acid methyl ester (PCBM), are crucial for its applications in organic thin film devices, such as organic solar cells and organic thin film transistors. In this work, the morphology, structural transformation, and crystallite orientation of PCBM film under thermal annealing as a function of annealing temperature, processing solvents, and solution concentrations are systematically investigated. Crystalline PCBM films with needle-like crystallites, axialitic aggregates, and faceted slices are formed in the annealing process. The axialites, made up of needle-like aggregates, are proposed to be partially developed spherulites frozen at the early growth stage formed through low-angle branching. The faceted slices are found to be PCBM single crystallites with hexagonal packing in the film plane. The film undergoes both amorphous-to-crystalline and crystalline-to-crystalline phase transformations as the annealing temperature is increased. The former transformation, corresponding to the self-organization of disordered PCBM molecules in the kinetically frozen films, occurs at a relative low temperature once the motion of these molecules is thermally activated, whereas the later one, corresponding to the transformation between two thermally stable crystalline phases, occurs when further increasing the annealing temperature. The PCBM crystallites composing these films are found to have an orientation preference normal to the film surface, which can be attributed to the confinement of film thickness for PCBM crystallite growth.

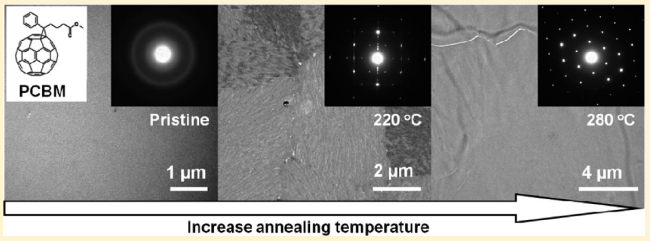

1. INTRODUCTION

Solution-processable organic electronic materials show great potential to achieve industrious applications because of their low cost and easy processability.[1] One major feature of the devices based on these materials lies on that the final device performance is not merely related to the intrinsic properties of the molecules but is also largely determined by the organization of the molecules within the active layer films.[2] It has been demonstrated that the overall crystallinity,[3] the shape,[4] and orientation[5] of the crystallites within the film, the molecular packing in the crystallites,[6] and the size and connectivity of the crystalline domains[7] all play quite important roles in determining the charge transport mobility. Unfortunately, the solution-processed films are usually amorphous or poor crystalline because of the fast and nonequilibrium film-forming process, leaving not enough time for the molecules to organize into ordered aggregates. Usually, highly crystalline films with larger domains, good connectivity between crystalline domains, and well-aligned crystallites are desirable for high-performance organic thin film transistors (OTFTs). Therefore, additional procedures have to be applied to manipulate the nanostructure of solution-processed films. For example, solvent annealing has been employed by Cho et al.[7] to increase the molecular ordering and field-effect mobility of OTFT devices based on soluble acenes, and it was shown that an increase of mobility over 100 fold had been achieved due to the increased overall film crystallinity and the formation of continuous crystals. By the assistance of postthermal annealing treatment and a vitrifying species, Stingelin et al.[8] have also realized controlled crystallization of solution-processed glassy rubrene thin films, resulting in a device mobility reaching 0.7 $cm^2\ V^{-1}\ s^{-1}$.

The soluble fullerene, [6,6]-phenyl-C_{61} acid methyl ester (PCBM), is one of the solution-processable n-type semiconducting materials showing considerable performance. It has been demonstrated that organic solar cells (OSCs) with PCBM as an acceptor have achieved a power conversion efficiency of over 5%[9] and OTFTs based on PCBM have also reached an electron mobility as high as 0.2 $cm^2\ V^{-1}\ s^{-1}$.[10−13] A large number of studies focusing on the morphology of OSC active layer films indicate that the nanoscale PCBM crystallites in PCBM/polymer blend films can facilitate electron transporting and are responsible for the enhancement of OSC efficiency.[14−16] Consequently, thermal annealing is frequently applied to promote the formation of PCBM crystallites in the device fabrication process. A close relation between the dimension of the resulting PCBM crystallites in the blend films and the annealing temperature, annealing time, and blending ratio has already been established.[17] However,

Received: April 1, 2011
Revised: May 16, 2011
Published: May 27, 2011

until now, no attention has been paid to morphology and nanostructural control of pure PCBM films, and the OTFT devices reported in the literature were almost based on as-spun grassy PCBM films without any additional treatment. Therefore, further effects focused on the molecular packing, crystallite size and orientation, film morphology, and the structural transformation of pure PCBM films are still in great demand.

This work attempts to promote the transformation of solution-processed pure PCBM films from the as-spun glassy state to the highly crystalline state with a controlled morphology. We try to establish a direct correlation between the morphology of the resulting films and the processing conditions, as well as to give a deeper understanding of the film nanostructure on aspects of molecular packing, crystallite orientation, and phase transformation. Therefore, thermal annealing was employed as the film-treating method, which resulted in highly crystalline PCBM films with needle-like crystallites, axialitic aggregates, and faceted slices. The film structure also underwent amorphous-to-crystalline and crystalline-to-crystalline phase transformations, respectively, as the annealing temperature was increased. It was also found that the crystallites composing the films showed a preferential orientation normal to the film surface.

2. EXPERIMENTAL SECTION

2.1. Materials. PCBM with a purity greater than 99% was purchased from Nichem Fine Technology Co. Ltd., Taiwan. *o*-Dichlorobenzene (oDCB, anhydrous, 99%) was purchased from Sigma-Aldrich Co., and chlorobenzene (CB, 99%) and chloroform (CF, 99%) were purchased from Beijing Chemical, China. All the solvents were used as received without further purification. The silicon wafers were cleaned in a piranha solution (70/30 v/v of concentrated H_2SO_4 and 30% H_2O_2) at 90 °C for 20 min, then thoroughly rinsed with deionized water, and finally blown dry in nitrogen.

2.2. Sample Preparation. First, PCBM solutions with concentrations of 10 and 20 mg/mL in CF, 20 mg/mL in CB, and 20 mg/mL in oDCB were spin-coated onto silicon wafers at 2000 rpm for 1 min. The residual solvent was then removed by storing the samples under vacuum for more than 12 h. At last, these films were placed on a hot plate at different temperatures for thermal annealing.

2.3. Characterization. Transmission electron microscopy (TEM), selected area electron diffraction (SAED), atomic force microscopy (AFM), out-of-plane X-ray diffraction (XRD), and differential scanning calorimetry (DSC) techniques were applied to characterize the morphology and structure of PCBM films.

For TEM characterization, the film was floated from a SiO_x/Si substrate with 10% HF solution and picked up with a copper grid. TEM images and SAED patterns were obtained with a JEOL JEM-1011 transmission electron microscope operated at an accelerating voltage of 100 kV.

AFM images were obtained using an SPA-300HV instrument with an SPI3800N controller (Seiko Instruments Inc., Japan) in tapping mode. A silicon microcantilevel (spring constant = 2 N/m, resonant frequency ≈ 70 kHz, Olympus, Japan) was used for the scanning.

Out-of-plane XRD measurement was performed using a Bruker D8 Discover Reflector (Cu Kα, λ = 1.54056 Å) with a generation power of 40 kV tube voltages and a 40 mA tube current operated in the locked couple mode.

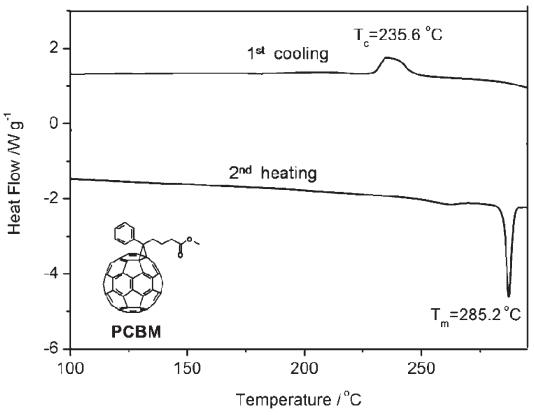

Figure 1. DSC thermograms showing heat flows of PCBM power. The inset is the chemical structure of PCBM.

DSC curves were performed on a TA Q100 DSC; both the heating and the cooling rates were set to 10 °C/min.

3. RESULTS AND DISCUSSION

In this work, first of all, we will demonstrate that thermal annealing is an effective method to manipulate the morphology of pure PCBM films and further show their morphological variations as a function of annealing temperature, processing solvent, and solution concentration. Especially, the formation and evolution of the resulting films with axialitic morphology will be well-discussed. The structural transformation corresponding to these morphological changes, including both the amorphous-to-crystalline and the crystalline-to-crystalline phase transformations, will be revealed. At last, the crystallites composing these films will be proved to be well orientated along the direction perpendicular to the film surface.

3.1. Annealed PCBM Thin Film Morphologies and Their Evolution Processes. The DSC curves in Figure 1 show that the melting point of PCBM is 285.2 °C, so the annealing temperature below 280 °C was selected to induce its cold crystallization. Figure 2 shows the AFM topography images of PCBM films processed from 20 mg/mL PCBM CF solution and further annealed at temperatures ranging from 140 to 260 °C. For the pristine film, a featureless surface with an rms roughness of 0.52 nm was obtained. After the film was annealed at 140 °C for 30 min, there was not any substantial change of the film topography except the slight increase of the film surface roughness to 0.64 nm. Above 140 °C, the surface roughness increased with the annealing temperature and lots of elongated aggregates appeared. As shown in Figure 2d, some tiny needle-like aggregates can be identified after annealing at 180 °C, which were imbedded in the amorphous part of the partly crystalline film and can be considered as PCBM crystallites. When the temperature was increased up to 200 °C (Figure 2e), for one thing, the entire film was occupied with PCBM aggregates and the film had been converted to a fully crystalline film; for another thing, the length and width of the aggregates became larger. The size of these aggregates further increased with the annealing temperature up to 260 °C. All these results prove that thermal annealing is an effective method to manipulate the morphology of PCBM films and, through thermal annealing, the solution-processed amorphous films can be transformed to highly crystalline films with size-controllable PCBM crystallites.

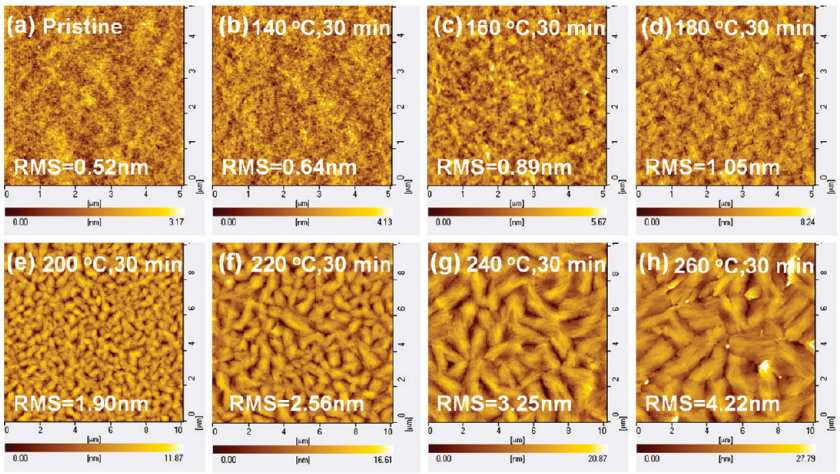

Figure 2. AFM topography images of PCBM films processed from 20 mg/mL PCBM CF solution and annealed at different temperatures for 30 min.

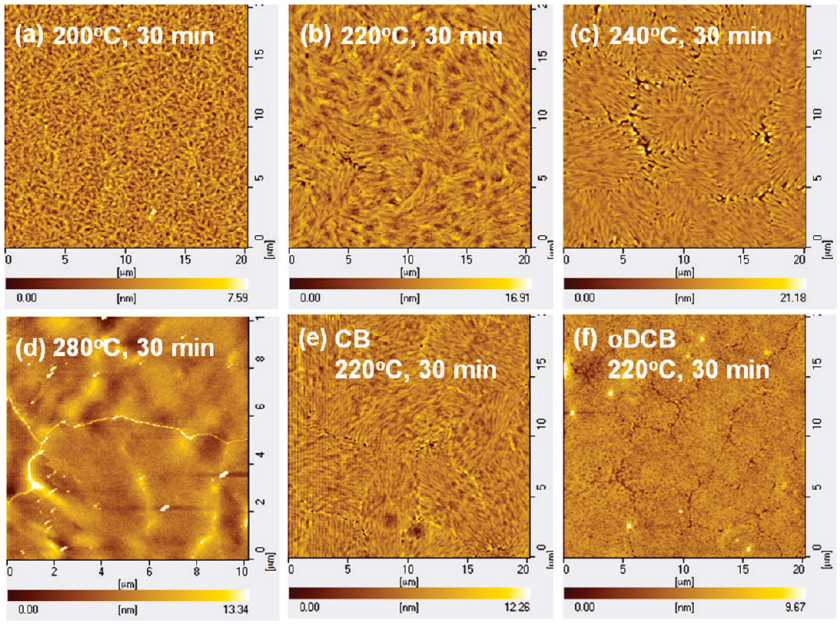

Figure 3. AFM topography images of annealed PCBM films processed from different solutions: (a−d) 10 mg/mL PCBM in CF, (e) 20 mg/mL PCBM in CB, and (f) 20 mg/mL PCBM in oDCB.

When PCBM films were processed from PCBM solution with lower concentrations or processed with higher-boiling-point solvents, although the pristine films were similar with Figure 2a, the annealed films showed different morphologies. Figure 3a−d shows the AFM topography images of PCBM films processed from 10 mg/mL PCBM CF solution and subsequently annealed at temperatures ranging from 200 to 280 °C. When annealed at 200 °C, the entire film was full of randomly oriented needle-like aggregates. In contrast, at 220 °C, the resulting film was composed of lots of microscaled domains made up of needle-like aggregates with short-range ordering. That morphology became more evident with the increases of both the domain size and the width of the needles when the temperature was increased up to 240 °C. However, this tendency did not continue as the temperature was further increased. As seen in Figure 3d, the domains composing the film annealed at 280 °C were faceted slices, suggesting that another type of PCBM crystallite maintaining a different structure from the needle-like crystallites may form at elevated temperature. Similarly, the films processed from 20 mg/mL PCBM solution with CB or oDCB as solvents and

Table 1. Surface Roughness and Thickness of Pristine PCBM Films Processed from PCBM Solutions with Different Solvents and Concentrations

solvent	CF		CB	oDCB
concentration (mg/mL)	20	10	20	10
rms roughness (nm)	0.518	0.653	0.485	0.461
film thickness (nm)[a]	82.6	40.3	37.0	18.1

[a] The thickness of the film was determined with an X-ray diffractometer in reflectivity mode.

dx.doi.org/10.1021/jp2030279 |J. Phys. Chem. B 2011, 115, 8071–8077

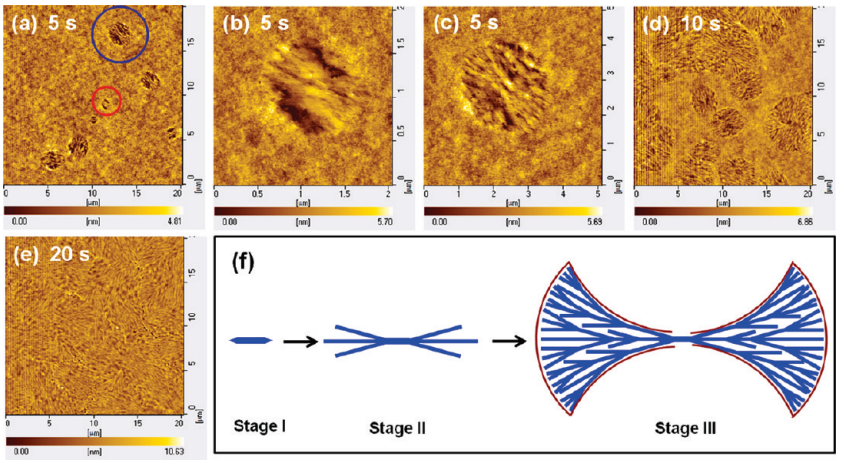

Figure 4. AFM topography images of PCBM films processed from 20 mg/mL PCBM CB solution and annealed at 220 °C for (a−c) 5 s, (d) 10 s, and (e) 20 s. (f) Schematic representation of the PCBM axialite evolution process. The circles in (a) indicate the selected area for zoomed-in AFM measurement in (b) and (c).

subsequently annealed at 220 °C (Figure 3e,f) possess the same microscaled domains containing needles, except for the differences of domain size and cracks formed between domains. Especially, large PCBM domains with a uniform size and clear needle-like aggregates can be formed when the film was processed from PCBM CB solution.

From these results, we can conclude that both the nature of processing solvents and the concentration of the PCBM solution show obvious effects on the morphology of annealed PCBM films. When the films were processed from 20 mg/mL PCBM CF solution, fluctuant films with small aggregates were formed after thermal annealing, whereas PCBM films with a flat surface and larger domains were formed when the films were processed from PCBM solutions with lower concentrations or with high-boiling-point solvents. We suggest that the film thickness and the initial aggregates in the pristine film are responsible for these differences. As shown in Table 1, when the film was processed from 20 mg/mL PCBM CF solution, the film thickness was 82.6 nm, whereas the film processed from 10 mg/mL PCBM CF solution or 20 mg/mL PCBM CB solution were much thinner (around 40 nm). In thicker films, upon annealing, PCBM aggregates not only develop in the plane of the film but also consume PCBM molecules in the vertical direction and develop upward. The transportation of PCBM molecules in the vertical direction results in a rougher film surface, whereas the higher density of PCBM aggregates in thicker films will lead to more intensive competition of crystallite growth and the exhaustion of amorphous PCBM molecules available for crystallite development at a much earlier stage, which will result in the formation of PCBM aggregates with a smaller size. In contrast, in thinner films, the development of PCBM aggregates in the vertical direction is largely suppressed by the limited film thickness and they can only develop in the film plane, resulting in films with a smoother surface and larger aggregates. Besides, the rms surface roughness is an indicator of the initial aggregates in pristine PCBM films. The larger rms surface roughness of PCBM films processed with CF as a solvent indicates that there are more initial aggregates in these films. The initial aggregates can act as a nucleus for PCBM aggregation, and more initial aggregates will also result in a higher density of PCBM aggregates with a smaller size.

We take great interest in the films formed at 220 °C. Because the domains composing these films have a 2-fold symmetry, we called them axialites, as described by Chen et al. when dealing with polymer crystallites produced from the melting state.[18] The feature of these crystallites lies on that these domains are not isotropic in all directions but maintain an axialitic morphology with favored growth in two opposite directions. To further investigate the nature of the axialitic aggregates and their evolution process, we followed the film developing process through conducting thermal annealing experiments at 220 °C for different times. As shown in Figure 4a−f, after 5 s of thermal treatment, there appeared to be some scattered small aggregates, which can be taken as the initial crystal nucleus. From the enlarged AFM images (Figure 4b,c) focusing on the crystal nucleus frozen at different developing stages, it can be concluded that, at the early stage of the crystal growth, the formed initial crystals have already gotten the axialitic morphology with the preferred growth direction along the long axis of the needle. At 10 s, their domain size has become much larger and over half of the film has been occupied. At 20 s, the entire film has been occupied with these polycrystalline domains and the film morphology does not undergo any changes if we further increase the annealing time up to 30 min. From the entire film developing process, we can conclude the following: First, the polycrystalline films are formed through the formation, development, and, eventually, the conjunction of isolated domains. Second, the crystallization of the film at 220 °C is really a fast process, which can be finished within 20 s. Third, once the final polycrystalline film is formed, it becomes quite thermally stable, which can maintain its morphology over 30 min under 220 °C.

On the basis of the evolution process of these PCBM axialitic aggregates and their growth habits, we believe that these axialites are partially developed spherulites frozen at the early growth stage. As seen in Figure 4f, in the beginning, PCBM tends to form needle-like single crystallites, which are similar to the crystallites formed at a lower annealing temperature in Figure 3a. The needles will then branch at their crystal growth fronts due to foreign particles or the lower molecular rotational mobility relative to the crystal interface propagation. Ultimately, the highly branched polycrystalline aggregates will develop to spherulites if their development continue. However, with the consumption of

dx.doi.org/10.1021/jp2030279 |J. Phys. Chem. B 2011, 115, 8071–8077

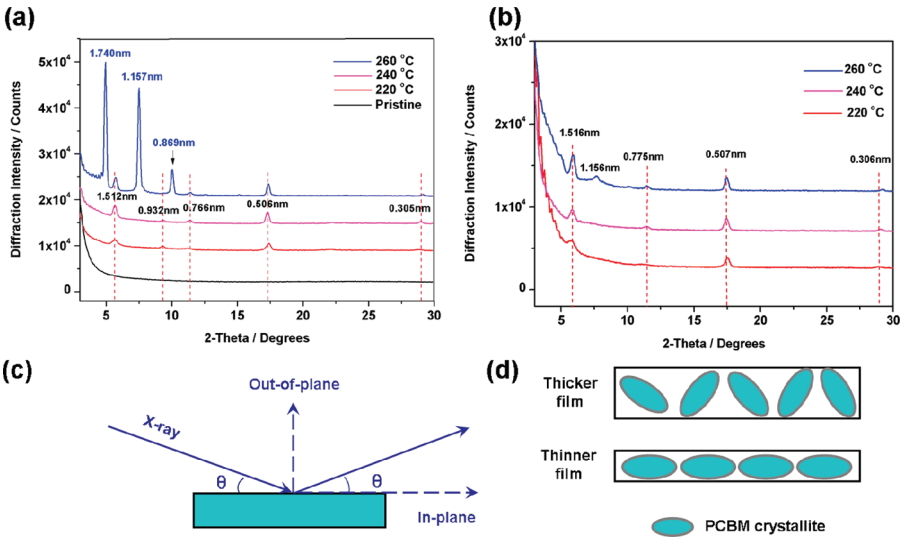

Figure 5. Out-of-plane XRD curves of PCBM films processed from (a) 20 mg/mL PCBM CF solution and (b) 20 mg/mL PCBM CB solution. Schematic representations of (c) the out-of-plane diffraction geometry and (d) the effect of film confinement on crystallite orientation.

PCBM molecules, these aggregates will collide into each other before the formation of spherulites, resulting in the ending of the polycrystalline growth at an early stage and the formation of axialites.

3.2. Two Structural Transformations of PCBM Thin Films. Figure 5a shows the X-ray diffraction curves of PCBM films processed from its 20 mg/mL CF solution and annealed at different temperatures. For the pristine film, no diffraction peaks were observed, which further confirms the amorphous nature of these films without any treatment. After thermal annealing at 220 °C, the five peaks corresponding to the *d*-spacings of 1.531, 0.934, 0.767, 0.507, and 0.307 nm indicate the amorphous-to-crystalline phase transformation of PCBM films. The crystalline phase of these films is referred to as phase I for easy clarification. The intensity of these peaks increases with annealing temperature, suggesting the enhanced overall crystallinity. When the annealing temperate has reached 260 °C, new sharp peaks with a strong intensity corresponding to the *d*-spacings of 1.740, 1.157, and 0.869 nm appear, which indicates that another PCBM crystalline phase (phase II) has been formed at that temperature. The annealed films processed from 20 mg/mL PCBM CB solution show similar diffraction curves (Figure 5b), except for the absence of the peak corresponding to the *d*-spacing of 0.934 nm, which may arise from the orientational changes of PCBM crystallites along the direction perpendicular to the film surface and will be discussed in detail in the section below.

When further enhancing the annealing temperature up to 280 °C, as seen in Figure 6, all the peaks corresponding to phase I disappear, indicating that all the crystallites formed at that temperature are in phase II. All the peaks in Figure 6 arise from the diffraction of the same crystal plane and can be indexed as (00*L*), assuming that the *c* axis of the crystal is perpendicular to the film surface. Besides, there are Laue oscillation peaks in the low-angle zone, from which the thickness of the film and the crystallites are estimated to be 37.93 and 32.92 nm, respectively, which indicates that the crystallites have almost penetrated throughout the entire film thickness. What's more, the film that has been first annealed at 240 °C and then at 280 °C shows the same diffraction curve as Figure 6, which indicates the direct

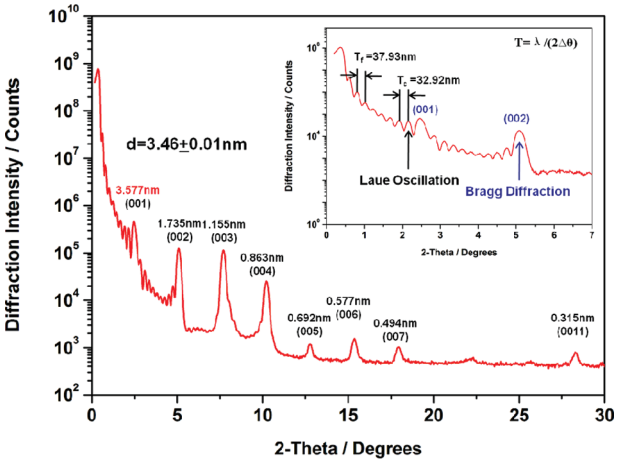

Figure 6. Out-of-plane XRD curves of PCBM films processed from 20 mg/mL PCBM CB solution and annealed at 280 °C for 30 min. The inset is an enlarged curve in the low-angle zone.

crystalline-to-crystalline phase transformation from phase I to phase II.

Figure 7 shows TEM images and the SAED patterns of several typical annealed PCBM films. For the pristine film, the TEM image in Figure 7a shows a uniform film without any large aggregation, which agrees well with the AFM image in Figure 2a. The SAED pattern of that film is a broad ring, which may arise from the scattering of nanoscale PCBM aggregates within that film, just as reported by Yang et al.[16] For the films annealed at 220 °C, the large aggregates appear in Figure 7b,c and their SAED patterns (Figure 7f,g) suggest the formation of PCBM crystallites. The diffraction ring corresponding to the *d*-spacing of 0.503 nm in Figure 7f agrees well with the diffraction points in Figure 7g, suggesting that the annealed PCBM films processed from different solvents maintain the same structure with different morphologies. Additional attention should be paid to Figure 7g, which shows the SAED pattern of a single PCBM domain as indicated in Figure 7d. For one thing, a single-crystal-like diffraction pattern is obtained, which suggests that the needle-like

dx.doi.org/10.1021/jp2030279 |*J. Phys. Chem. B* 2011, 115, 8071–8077

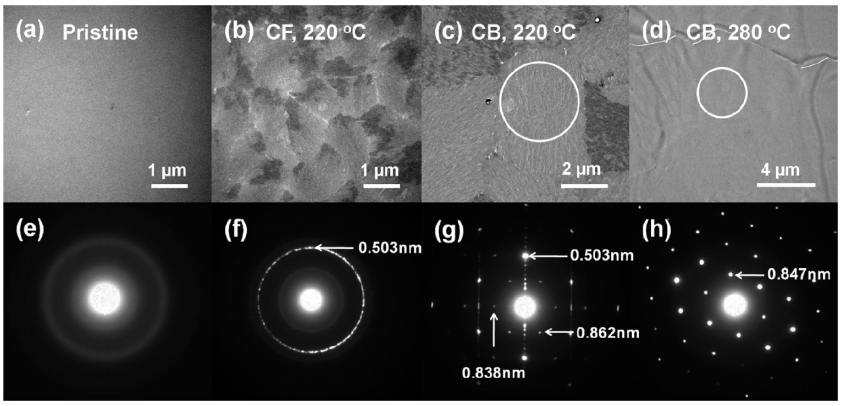

Figure 7. TEM images of PCBM films (a) without thermal treatment, (b) processed from 20 mg/mL PCBM CF solution and annealed at 220 °C, (c) processed from 20 mg/mL PCBM CB solution and annealed at 220 °C, and (d) processed from 20 mg/mL PCBM CB solution and annealed at 280 °C. Panels e−h are the corresponding SAED patterns. The circles in (c) and (d) indicate the selected areas for SAED characterization.

crystallites within that domain are locally orientated in both in-plane and out-of-plane directions. For another thing, there are lots of close-arranged diffraction points along the long axis of these needles and the *d*-spacing corresponding to these points can be expressed as $(0.503/n) \times 11$ nm ($n < 11$). Although we do not understand the exact origin of these diffraction points, we suggest that these diffraction points arise from a supramolecular structure within these needles, which may imply a more intensive intermolecular interaction between PCBM in these crystallites than expected. When the annealing temperature is 280 °C, the SAED pattern in Figure 7h confirms that these faceted domains are indeed PCBM single crystals holding a hexagonal molecular ordering in-plane with a maximum *d*-spacing of 0.847 nm. All the TEM images and SAED patterns agree well with the XRD data and further confirms the crystalline-to-crystalline phase transformation.

3.3. Crystalline PCBM Thin Film Orientation. Recently, Bao et al.[19] have investigated the crystallization of PCBM thin films under thermal annealing with an in situ grazing incidence X-ray scattering (GIXS) technique. They found that the crystallites had a preferential orientation relative to the substrate and the orientation of these crystallites was attributed to the heterogeneous nucleation at the film/substrate interface. Herein, through thermal annealing at higher temperature (over 200 °C) with films of varied thicknesses, we have also observed such an orientation preference of PCBM crystallites and we suggest that additional factors, such as the geometrical shape of PCBM crystallites and the spatial confinement of the film, may also be responsible for that feature.

The XRD curves in Figure 5a,b show that, when the thickness of PCBM films has been changed from 82.6 to 37.0 nm, the peaks corresponding to the *d*-spacing of 0.932 nm are absent while the other peaks still maintaining their positions. The left peaks in Figure 5b corresponding to the *d*-spacings of 1.525, 0.774, 0.507, and 0.307 nm can be indexed as the first-, second-, third-, and fifth-order diffractions of the same crystal plane of PCBM crystallites in phase I, indicating that the crystallites within that film maintain a unique crystal axis perpendicular to the film surface. The single-crystal-like SAED pattern of a single axialite in Figure 7g further confirms that these crystallites maintain a constant crystal plane parallel to the film surface. Therefore, the absence of diffraction peaks in thinner films indicates that, as the film thickness is decreased, PCBM crystallites align better in the film plane. Because the PCBM axialites are composed of elongated needle-like crystallites, in the crystallization process, the needle-like structures tend to develop with their long axes in the film surface plane and the development normal to the film surface is largely suppressed by the confinement of the film thickness, resulting in the crystallization orientation preference mentioned above. As seen in Figure 5d, the spatial confinement effect of the film decreases with the increase of the film thickness; therefore, the crystallites in the relatively thicker film processed from 20 mg/mL PCBM CF solution do not align well, which explains the additional diffraction peak corresponding to the *d*-spacing of 0.934 nm in its X-ray diffraction curve in the out-of-plane direction (Figure 5a). From the indexed X-ray diffraction peaks (Figure 6) and the hexagonal SAED pattern (Figure 7h) of the faceted crystallites formed at 280 °C, we can infer that these crystallites also have a preferential orientation along the out-of-plane direction. Because the crystallites formed at 280 °C tend to form 2D slices with their plane parallel to the film surface, we believe that, in the crystallizing process, only the initial crystal nuclei with their *c* axis perpendicular to the film surface can survive and have the chance to develop into microscaled crystallites.

4. CONCLUSIONS

In this work, both the morphology and the structural dependences of PCBM thin films upon thermal annealing were well-investigated. It was found that, as the annealing temperature was increased, the aggregates composing the film changed from elongated needle-like crystallites to axialitic domains and finally to faceted crystalline slices. The nature and evolution process of these axialites were revealed, and they were found to be actually the partially developed spherulites frozen at the early growth stage. The size of these axialites was determined not only by annealing temperature but also by the film thickness and the amounts of initial nuclei within the pristine films. Larger axialites can be obtained with thinner films that contain fewer initial nuclei. At the same time, the film structure also underwent amorphous-to-crystalline and crystalline-to-crystalline phase transformations as the annealing temperature increased. The former transformation corresponding to cold crystallization occurred at a relatively lower temperature once the motion of PCBM molecules was motivated, whereas the latter transformation occurred when the

annealing temperature was further increased up to 280 °C. The crystallites with both crystalline phases were preferentially oriented in the out-of-plane direction, which may be attributed to the combined effects of the geometrical shape of PCBM crystallites and the spatial confinement of the film.

AUTHOR INFORMATION

Corresponding Author
*Tel: 86-431-85262175. Fax: 86-431-85262126. E-mail: ychan@ciac.jl.cn.

ACKNOWLEDGMENT

This work was financially supported by the National Natural Science Foundation of China (20621401, 20834005, 51073151) and the National Basic Research Program of China (973 Program-2009CB930603).

REFERENCES

(1) Dimitrakopoulos, C. D.; Malenfant, P. R. L. *Adv. Mater.* **2002**, *14*, 99.
(2) Liu, S. H.; Wang, W. C. M.; Briseno, A. L.; Mannsfeld, S. C. B.; Bao, Z. N. *Adv. Mater.* **2009**, *21*, 1217.
(3) Chang, J. F.; Sun, B. Q.; Breiby, D. W.; Nielsen, M. M.; Solling, T. I.; Giles, M.; McCulloch, I.; Sirringhaus, H. *Chem. Mater.* **2004**, *16*, 4772.
(4) Yang, H. C.; Shin, T. J.; Ling, M. M.; Cho, K.; Ryu, C. Y.; Bao, Z. N. *J. Am. Chem. Soc.* **2005**, *127*, 11542.
(5) Becerril, H. A.; Roberts, M. E.; Liu, Z. H.; Locklin, J.; Bao, Z. N. *Adv. Mater.* **2008**, *20*, 2588.
(6) Ji, H. X.; Hu, J. S.; Wan, L. J.; Tang, Q. X.; Hu, W. P. *J. Mater. Chem.* **2008**, *18*, 328.
(7) Lee, W. H.; Kim, D. H.; Cho, J. H.; Jang, Y.; Lim, J. A.; Kwak, D. K.; Cho, K. *Appl. Phys. Lett.* **2007**, *91*, 092105.
(8) Stingelin-Stutzmann, N.; Smits, E.; Wondergem, H.; Tanase, C.; Blom, P.; Smith, P.; de Leeuw, D. *Nat. Mater.* **2005**, *4*, 601.
(9) Chen, H. Y.; Hou, J. H.; Zhang, S. P.; Liang, Y. Y.; Yang, G. W.; Yang, Y.; Yu, L. P.; Wu, Y.; Li, G. *Nat. Photonics* **2009**, *3*, 649.
(10) Singh, T. B.; Marjanovic, N.; Stadler, P.; Auinger, M.; Matt, G. J.; Gunes, S.; Sariciftci, N. S.; Schwodiauer, R.; Bauer, S. *J. Appl. Phys.* **2005**, *97*, 083714.
(11) Cho, S.; Seo, J. H.; Lee, K.; Heeger, A. J. *Adv. Funct. Mater.* **2009**, *19*, 1459.
(12) de Haas, M. P.; Warman, J. M.; Anthopoulos, T. D.; de Leeuw, D. M. *Adv. Funct. Mater.* **2006**, *16*, 2274.
(13) Anthopoulos, T. D.; Tanase, C.; Setayesh, S.; Meijer, E. J.; Hummelen, J. C.; Blom, P. W. M.; de Leeuw, D. M. *Adv. Mater.* **2004**, *16*, 2174.
(14) Reyes-Reyes, M.; Lopez-Sandoval, R.; Arenas-Alatorre, J.; Garibay-Alonso, R.; Carroll, D. L.; Lastras-Martinez, A. *Thin Solid Films* **2007**, *516*, 52.
(15) Reyes-Reyes, M.; Kim, K.; Dewald, J.; Lopez-Sandoval, R.; Avadhanula, A.; Curran, S.; Carroll, D. L. *Org. Lett.* **2005**, *7*, 5749.
(16) Yang, X. N.; van Duren, J. K. J.; Rispens, M. T.; Hummelen, J. C.; Janssen, R. A. J.; Michels, M. A. J.; Loos, J. *Adv. Mater.* **2004**, *16*, 802.
(17) Swinnen, A.; Haeldermans, I.; vande Ven, M.; D'Haen, J.; Vanhoyland, G.; Aresu, S.; D'Olieslaeger, M.; Manca, J. *Adv. Funct. Mater.* **2006**, *16*, 760.
(18) Chen, S. H.; Su, A. C.; Chen, S. A. *Macromolecules* **2006**, *39*, 9143.
(19) Verploegen, E.; Mondal, R.; Bettinger, C. J.; Sok, S.; Toney, M. F.; Bao, Z. N. *Adv. Funct. Mater.* **2010**, *20*, 3519.